engineering proceedings

MDPI

Proceeding Paper

Electrostatic Surface Functionalization of Physical Transducers of (Bio)Chemical Sensors: Thiocyanate-Modified Gold Interface †

Borys A. Snopok [1,2,*], Arwa Laroussi [1], Tetyana V. Snopok [2] and Shavkat Nizamov [1]

[1] Nanobiotechnology—Institute of Biotechnology, Brandenburg Technical University Cottbus-Senftenberg, Universitätsplatz 1, 01968 Senftenberg, Germany; laroussiarwa1@gmail.com (A.L.); nizamov@b-tu.de (S.N.)
[2] Optoelectronics—V.E. Lashkaryov Institute of Semiconductor Physics, National Academy of Sciences of Ukraine, 41 pr. Nauki, 03028 Kyiv, Ukraine; t_snopok@yahoo.com
* Correspondence: snopok@isp.kiev.ua
† Presented at The 11th International Electronic Conference on Sensors and Applications (ECSA-11), 26–28 November 2024; Available online: https://sciforum.net/event/ecsa-11.

Abstract: Immobilization of functional nano-blocks by means of electrostatic interactions is a promising technology for creating sensitive layers of (bio)chemical sensors. This is due to the unique ability of electrostatic interactions to directional immobilization and uniform distribution of charged objects over the surface. This report discusses methods for introducing an electrostatically active buffer layer onto the gold surface and studies its interaction with nanoparticles carrying charges of different signs on their surface. To study the adsorption capacity of the gold surface modified with thiocyanate, silver nanoparticles of 60 nm in size, stabilized by positively charged Ag-NP&BPEI and negatively charged Ag-NP&CIT, Ag-NP&PEG and Ag-NP&PVP, were used as an electrostatic probe. Analysis of SPR and UV-VIS spectroscopy results, electrochemical measurements and wide-field surface plasmon resonance microscopy imaging indicate that the gold surface modified with thiocyanate behaves as a negatively charged object in processes drive by electrostatic interactions.

Keywords: silver nanoparticles; surface plasmon resonance (SPR); polymer coating; bio(chemical) sensors; thiocyanate; surface charge; electrostatic interaction; wide-field surface plasmon resonance microscopy; cyclic voltammograms

Citation: Snopok, B.A.; Laroussi, A.; Snopok, T.V.; Nizamov, S. Electrostatic Surface Functionalization of Physical Transducers of (Bio)Chemical Sensors: Thiocyanate-Modified Gold Interface. *Eng. Proc.* **2024**, *5*, x. https://doi.org/10.3390/xxxxx

Academic Editor(s): Name

Published: 26 November 2024

1. Introduction

Conventional wisdom holds that the limitations associated with the performance of modern (bio)chemical sensors are primarily due to the sensing layer [1]. To achieve maximum efficiency, the sensing layer must not only recognize the target analyte but also enable the physical transducer to realize high sensitivity and achieve the lowest possible detection limit. It is particularly important for transducer-based biosensors (e.g., Surface Plasmon Resonance, SPR) owing to the complex interplay between the affinity reactions that give rise to the response and the spatial distribution of the recognition architecture on the transducer surface [2,3]. This is due to the exponential decay in the intensity of the evanescent wave, the test radiation of the SPR sensor: processes in the area of intersection of spaces occupied by the evanescent wave and sensitive architecture are the source of the sensor's information signal [3]. To fabricate high-performance SPR sensors, it is often desirable to deposit a thin recognition layer because analytical efficiency is highly dependent on this layer's thickness [4]. However, creating an ultra-thin buffer layer between the metal surface and functional recognition centers of biological origin is a complex task: on the one hand, this layer must prevent the destructive effect of the underlying gold on the

secondary and tertiary structure of proteins, and on the other hand, it must ensure targeted spatially oriented immobilization of the necessary bioreceptors.

Self-assembly of specialized nanoparticles, biological macromolecules, nanoparticle conjugates with biorecognition sites, etc. into a single sensor architecture is only possible if this buffer layer facilitates the direct and targeted integration of nanoscale building blocks and, hence, transforming them into feasible analytical platform. This is strongly related to the ability to control the interfacial assembling and the quality of the association between the functional units and the surface through the variation of the macroscopic environment (pH, ionic strength, external electric field etc.). Current thrusts are towards strategies that dynamically assemble functional units around which the environment is purposefully structured at the nanoscale, the level at which the molecular recognition function is formed. Within this framework, our interest is focused on finding routes to incorporate electrostatically-active buffer layer onto metal surfaces in order to control the interplay of interfacial forces retaining of biological recognition units near the surface.

Surface charging has been widely used in various functionalization technologies to create (bio)chemical sensing layers. This is due to the unique ability of electrostatic interactions not only to immobilize the desired receptors, but also to cause their uniform distribution over the surface owing to in-plane electrostatic repulsion (the value of which can be controlled by the ionic strength of the surrounding solution). Self-assembling protocols based on self-limiting aggregation of electrostatic arrays are widely used in sensor science from classical layer-by-layer deposition [5,6] to electrostatic levitation of proteins over the surface of thiocyanate-modified gold [7]. First proposed in ref. [8], thiocyanates are extremely promising compounds for creating an ultrathin buffer layer on the surface of SPR, QCM, etc. transducers, due to their small size and ability to self-organize into a monolayer on the surface of gold.

Despite the apparent simplicity of thiocyanate structure (complex compounds with the $^{-}S{-}C{\equiv}N$ or $S{=}C{=}N^{-}$ anion), they continue to be the subject of active scientific debate. This is due to disagreement regarding the presence of equilibrium tautomeric forms of thiocyanic acid [9], the composition of their complexes with metals (i.e., Au(SCN)x) [10], the possibility of polymerization [11], etc. For sensor science, an important issue is the experimental confirmation of the presence of the supposed effective negative charge of their self-organizing monolayer. This study is devoted to the investigation of this issue.

2. Materials and Methods

Chemical (hydrochloric acid (HCl, 37%), hydrogen peroxide (H_2O_2, 30%), H_2SO_4 (37%), acetone, ethanol, isopropanol, NaCl, glycine, GuaSCN) reagents were purchased from Sigma-Aldrich. Stock solution of 60 nm silver nanoparticles coated with CITrate anions (Ag-NP&CIT, "60 nm Citrate nanoXact silver", DMW0035, 0.02 mg/mL), large Poly-Vinyl-Pyrrolidone polymer (Ag-NP&PVP, "60 nm PVP nanoXact silver", ECP1046, 0.02 mg/mL), non-ionic Poly(Ethylene Glycol) (Ag-NP&PEG, "60 nm PEG nanoXact silver", JCP1111, 0.02 mg/mL) and Branched-Poly-EthylenImine (Ag-NP&BPEI, "60 nm BPEI nanoXact silver", MRL1009, 0.02 mg/mL) were purchased from nanoComposix (www.nanocomposix.com). All suspension and regeneration solutions were prepared according to the standard procedures using Milli-Q-purified water (55 μS/cm) in small glass vials 10 mL. Working suspension of Ag NP were prepared from the stock solution immediately before conducting measurements.

In line with producer specification (www.nanocomposix.com accessed on 18 November 2024) in distilled water with a pH of 5.5-6, the charge of these compounds changes from the strongly positively charged Ag-NP&BPEI (conferred by 25 kDa BPEI with active primary, secondary and tertiary amino groups; ζ-potential is c.a. +60 mV at pH 6), through Ag-NP&PEG (conferred by 5 kDa PEG with active −OH groups, ζ-potential is c.a. −30 mV at pH 6), and Ag-NP&PVP (conferred by 40 kDa PVP with cyclic 5-membered 2-Pyrrolidone, ζ-potential is c.a. −40 mV at pH 6) with a moderate negative charge, to the highly

negatively charged Ag-NP&CIT (conferred by citric acid with active carboxylic groups, ζ-potential is c.a. −50 mV at pH 6).

The SPR chip support was made of a glass plate (n = 1.61) with dimensions of 20 × 20 × 1 mm^3. For the gold film fabrication, the upper side of the plate was covered with a ~5 nm adhesive layer of chromium followed by a 50 ± 3 nm of gold using thermal evaporation in vacuum (the evaporation rate c.a. 4–5 nm/s). The resulting films are polycrystalline gold with an average crystallite size of about 30 nm and a root-mean-square roughness not exceeding several nanometers [12]. Immediately before use, the chips were cleaned of organic contaminants using the Piranha treatment (40–50 s), then after rinsing in distilled water, they were subjected to chemical nanopolishing in 3% HAHP ({3 mL}HCl:{3 mL}H_2O_2:{94 mL}H_2O ($v/v/v$), see ref. [13] for details). After the treatment, the chips were washed in distilled water and dried in a stream of dry air.

The UV-VIS spectra of samples were recorded using an Evolution 220 spectrometer (Thermo Fisher Scientific GMBH, Dreieich, Germany). For the monitoring of the extinction of films, the SPR chips were cut into fragments of the c.a. 5 × 20 mm^2 size and placed close to the inner surface of the 10 mm glass cuvettes. Measurements were carried out in differential mode relative to the corresponding reference sample unless otherwise stated.

Cyclic voltammograms of gold films (used as working electrodes) were recorded using a conventional three-electrode setup with contacts for large area film samples (see ref. [13] for details). Au polycrystalline films (part of the commercial SPR chips, typically 10 × 20 mm^2) were used as working electrodes; a platinum wire of 0.25 mm in diameter was used as the counter electrode, and an Ag/AgCl (a saturated KCl) electrode with a double salt bridge (Metrohm) was used as the reference electrode. All electrochemical measurements were performed using PC-controlled Autolab PGstat12 equipped with a FRA32 impedance module and controlled by NOVA 2.1.2 software (Metrohm, www.metrohm.com) at room temperature with additional deaeration (bubbling by N_2 during 3 min) of 0.05 M of H_2SO_4 in water.

An SPR spectrometer "Biosupplar" with angular scanning and a GaAs laser as the source of excitation (at a wavelength of 650 nm) [14] was used. The SPR chips were fixed to a supporting glass prism (refractive index 1.61) with an immersion liquid. The measurements were performed in the flow mode with peristaltic pump connected after the measuring cell. For measurements, a complete scan mode with SPR curve registration was used; the dependence of SPR minimum on time have been registered for kinetics analysis.

The SPR chips were cleaned and modified off- or online as indicated in the text below. After a stable baseline value was established beyond etching and modification procedures, the cell was perfused by distilled water, then by suspension of Ag nanoparticles. After 15–20 min or more, it was washed with water. If necessary, after binding NP was removed by perfusion of aqueous solution containing 3M NaCl, 10 mM Glycine pH 2.0 or EDTA for 5–10 min. Then the cell was washed with water again.

The setup for wide-field Surface Plasmon Resonance Microscopy (wf-SPRM) described in ref. [15,16] in details. Shortly, light from 642 nm SM-fiber coupled laser diode (with current and temperature control) was collimated by the length objective and directed through free aperture Glan polarizer set to the p-polarization on the gold coated prism surface. Gold coated sensors consist of SF-10 (n = 1.72) glass prisms with 43–45 nm gold layer on 3–5 nm titanium adhesive layer. The measurements were performed at the angle 0.1–0.3 degrees before SPR minimum. The image was formed on a CMOS image sensor with 2592 × 1944 pixels resolution (field of view of c.a. 1.5 mm^2) at ~15 frames per second. For data collection and further analysis has been done by the homemade software, see ref. [17] for details.

3. Results and Discussion

Initial study was focused on the changes in the extinction spectra of NP suspensions after keeping a SCN-modified gold film in their volume in the dark for 20 h. The stock solutions were diluted 10 times with distilled water, and a fragment of a gold SPR chip

with an area of about 5 × 20 mm² was immersed in such a working solution. Dilution was used to reduce the number of particles so that their adsorption led to a noticeable change in the spectrum of the solution. The results of these experiments are shown in Figure 1; when recording these spectra, the gold plate was positioned so that the beam of the spectrophotometer did not fall on it. The data presented in the figures indicate that only in the case of Ag-NP&BPEI did the concentration of particles in the solution decrease significantly.

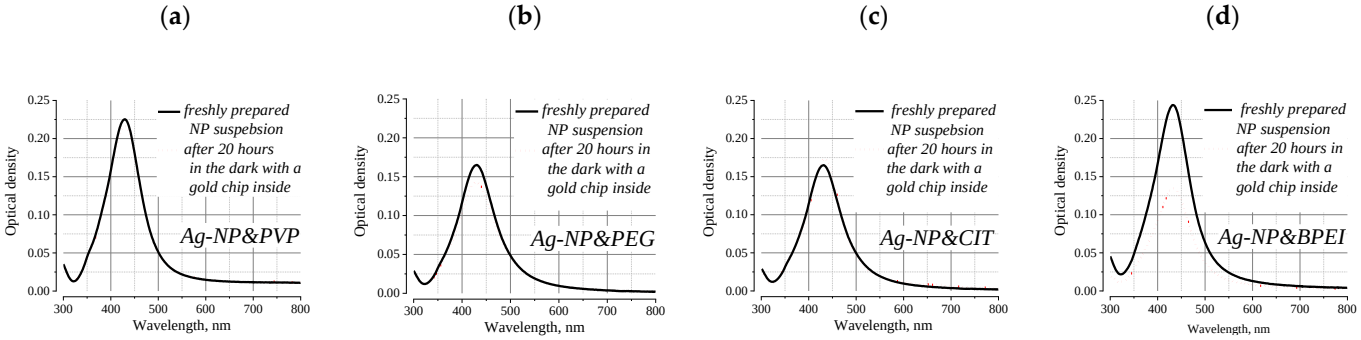

Figure 1. Dependence of extinction of aqueous solutions of silver nanoparticles with a diameter of 60 nm, stabilized by organic shells based on PVP (**a**), PEG (**b**), CIT (**c**) and BPEI (**d**), before (solid line) and after (dashed line) immersion of a gold plate with a total area of about 5 × 20 mm² in their volume (5 mL) for 20 h in the dark. The concentration of nanoparticles in 10 mL glass vials was about 0.002 mg/mL (according to the manufacturer's specification after diluting the stock solution 10 times with distilled water).

However, additional experiments showed that the adsorption of Ag-NP&BPEI occurs not only on the gold surface, but also on the wall of the glass cuvette and on the back (glass) surface of the gold plate; the number of adsorbed nanoparticles on the SPR chip and the walls of the glass cuvette turned out to be comparable in quantity (). For the Ag-NP&PVP, Ag-NP&PEG and Ag-NP&CIT suspensions, such an effect is not observed.

The published data on both BPEI-coated nanoparticles and the water-soluble BPEI /PEI polymer itself are in good agreement with the obtained result. Numerous studies have shown that BPEI has excellent adhesive properties to any solid substrate [18]. High-molecular branched PEIs containing primary, secondary and tertiary amino groups fixed at highly flexible chains organized in a large free volume are an excellent adhesion-enhancing layer due to their good adhesion to metals [19], charged polyelectrolytes [20] and biomaterials, including living cells [21] through van der Waals or ion-polar group interactions. Such diverse capabilities of BPEI for interfacial reactions suggest the need for additional experimental studies to clarify the dominant effect during interaction with a thiocyanate-modified gold surface.

To verify the presence of Ag NP on the SCN-modified gold surface we performed cyclic voltametric (CV) measurements [22]. CV measurements quantify the electrochemical accessibility of the surface and provide complementary information about the presence of other than materials of working electrode active crystals/compounds on the electrode surface [23].

To exclude artefacts gold slides freshly rinsing with the solvents, treated in "Piranha" to remove organic residues and nano-polished in 3% HAHP [13] before thiocyanate treatment were used, recording three cycles in total (Figure 2). Data from the first cycle was used to evaluate the surface properties (Figure 2a). Cyclic voltammograms were taken for standard SPR gold chip after treated respectively for Ag-NP&BPEI, Ag-NP&CIT, Ag-NP&PEG and Ag-NP&PVP suspensions in distilled water (for several hours to ensure that a steady filling is achieved, NP's concertation is above 0.002 mg/mL).

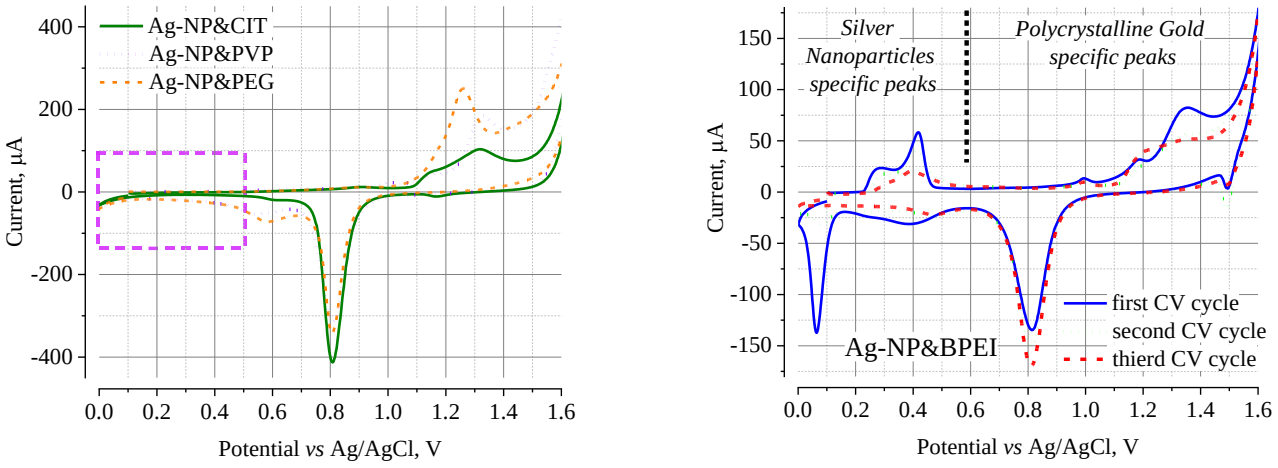

Figure 2. Cyclic voltammograms recorded at scan rate 50 mV/s recorded for a polycrystalline gold electrode with previously adsorbed citrate CIT, PVP, PEG (**a**) and BPEI (**b**) stabilized silver nanoparticles 60 nm in diameter in 0.05 M H_2SO_4 at 25 °C in a conventional three-electrode cell setup.

The CV after immersion of thiocyanate modified polycrystalline gold in Ag-NP&CIT, Ag-NP&PEG and Ag-NP&PVP water suspensions (Figure 2a) does not differ significantly for a native gold electrode discussed by us in ref. [13]. Shortly, a peak/shoulders of oxidative current at 1.18 and 1.23 V as well as peak of reductive currents at 0.81 V are observed; overlapping oxidation peaks indicates the main contribution to originate from the (100) surface with some variations typical for the polycrystalline layers. In general, it can be stated that adsorbed silver nanoparticles on the gold surface could not be registered for samples immersed in Ag-NP&CIT, Ag-NP&PEG and Ag-NP&PVP water suspensions.

The cyclic voltammogram of thiocyanate modified gold electrodes treated for Ag-NP&BPEI suspension has a number of quantitative and qualitative differences from the samples considered above. First of all, the current value typical for similar unmodified gold electrodes (see ref. [13]) as well as samples in Figure 2a a is significantly reduced. For example, the reducing part of the CV with an intense peak at 0.81 V decreases more than 3 times. According to ref. [13], the intensity of this peak can be used as an indicator of the amount of surface-active gold atoms. A comparison of this reduction charge with total number of gold atoms on the cleaned surface indicates that over 50% of the surface gold atoms are involved into this process; after adsorption of Ag-NP&BPEI, this value decreases to less than 20%.

The peaks of the cyclic voltammogram in the region from 0.0 to 0.6 V are probably for silver nanoparticles. The observed anodic peaks at 0.27 and 0.42 V and the cathodic peak at ~0.07 V (Figure 2b) could be attributed to silver nanoparticles: the obtained values are close to those observed in [24,25]. This allows us to confirm the above conclusion that Ag-NP&BPEI form an adsorbed layer on the surface of gold modified with thiocyanate.

It is also interesting to emphasize the well-known fact that due to the high electrochemical activity of silver nanoparticles, they actively dissolve during subsequent cycling [26]. Thus, for example, after the third cycle, the characteristic peaks of silver practically disappear (Figure 2b). As expected, the intensity of the reductive part of the CV with the strong peak at 0.81 V increases as access to the surface gold atoms increases. The magnitude of this peak is still smaller than that of the original gold electrode, probably because organic fragments of the branched polyethyleneimine polymer with positively charged groups still cover most of the electrode owing to mentioned above high adhesion of BPEI polymer to any solid support.

Classical angle-scanning surface plasmon resonance spectroscopy was used to directly monitor the adsorption process of nanoparticles on a thiocyanate-modified gold surface [27,28]. Figure 3a shows the SPR response for a typical workflow with on-line cleaning, surface modification with thiocyanate, and subsequent adsorption of the nanoparticle suspension. The results of the study show that PEG-coated silver nanoparticles are practically not adsorbed on the gold surface, and their response on the thiocyanate-modified surface is small. Ag-NP&PVP show an adsorption response on the unmodified gold surface (a few hundredths of a degree) and do not bind at all to the thiocyanate-modified surface. In general, it can be stated that the adsorption properties of these NPs are due to the structure of the water-soluble polymers covering these nanoparticles: the labile nature of the PEG chains prevents their adsorption on the gold surface, while both the van der Waals forces and charge transfer interactions characteristic of the large surface area of PVP stimulate the binding of Ag-NP&PVP to the gold surface.

The response of the SPR sensor with an unmodified gold surface on injection of Ag-NP&CIT and Ag-NP&BPEI is similar for both suspensions (c.a. +0.012° in 15 min, Figure 3b). When interacting with unmodified gold, the adsorption of both CIT and BPEI-coated nanoparticles is driven by the chemical functionality of the polymers rather than electrostatic interactions. Indeed, X-ray photoelectron spectroscopy shows that the BPEI layer interacts with the Au surface via polar/ionic groups and van der Waals interactions [19]. In this case, the nitrogen atom of the amino group act as an electron pair donor to chelate the metal atoms.

The SPR response characteristics for the adsorption of Ag-NP&CIT and Ag-NP&BPEI on the SCN-modified gold surface are significantly different from those discussed above for the unmodified gold surface (Figure 3b). While the addition of Ag-NP&CIT leads to a small «negative» response (decrease in the angle at which the SPR is observed), the interaction of Ag-NP&BPEI nanoparticles with the surface leads to a monotonic increase in the magnitude of the «positive» response for at least several hours (Figure 4). It should also be noted that when storing samples in air, some changes in the properties of the thiocyanate coating are observed (Figure 3b), but this does not affect their qualitative behavior in terms of the nature of adsorption processes.

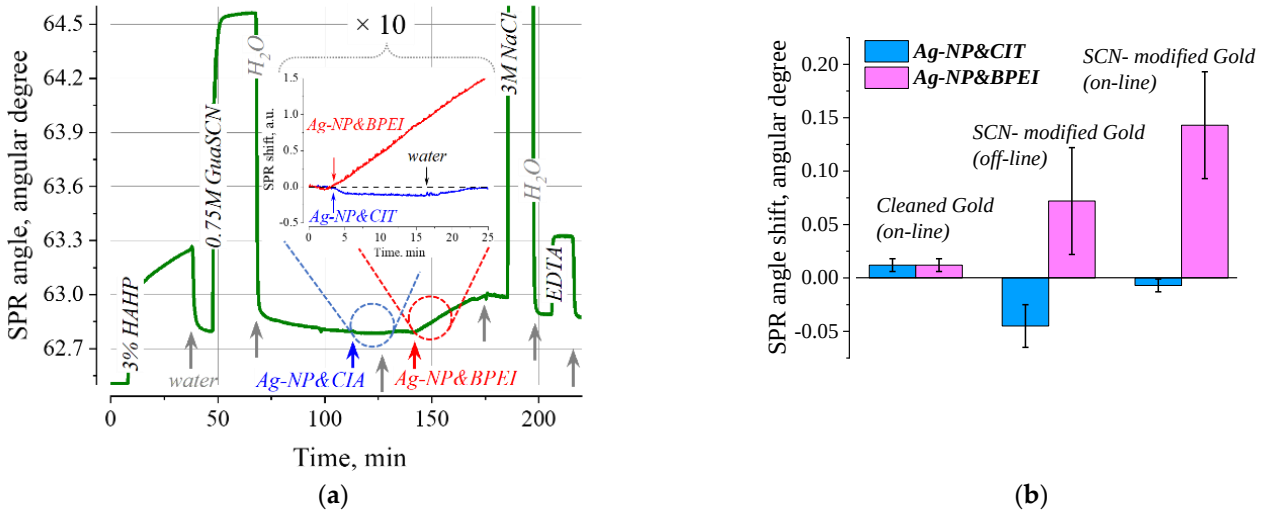

Figure 3. Typical SPR sensing of Ag nanoparticle adsorption (**a**) and its responses achieved after 15 min on the various surfaces (**b**). The SPR chips were cleaned in Piranha solution immediately before measurements, "on–line" nanopolished in 3% HAHP and modified by thiocyanate (0.75 M GuaSCN) in distilled water at room temperature immediately after the mounting in the instrument. The insert illustrates specific SPR responses on Ag-NP&CIT and Ag–NP&BPEI injection with 10 times magnification. The "off-line" samples were prepared in advance, unlike the "on-line"

samples, the purification and modification of which was carried out in a single experiment with the adsorption reaction (as illustrated in Figure (**a**)).

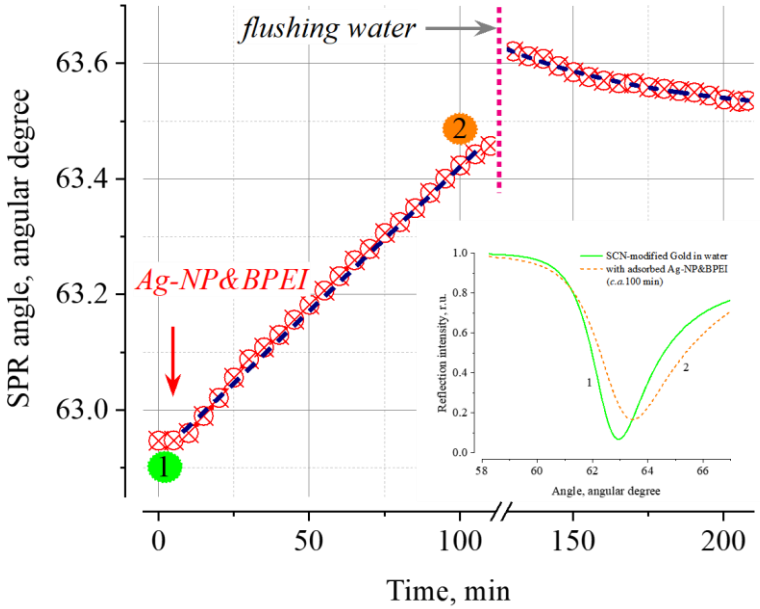

Figure 4. Kinetics of SPR angle during adsorption of Ag-NP&BPEI nanoparticles from water suspension (the "on-line" samples). The dashed lines serve as eye guides. The curves in the inset illustrate the dependences of the reflection intensity on the angle of incidence of laser radiation on the interface of the SPR chip before and after adsorption of silver nanoparticles with the BPEI shell.

The results presented in Figure 3 and 4 allow us to conclude that silver nanoparticles with a positively charged BPEI coating at a given pH value interact with the SCN-modified surface of the SPR transducer, significantly changing the magnitude of its response. The observed dependences for positively charged Ag-NP&BPEI obviously cannot be interpreted within the framework of the classical adsorption model, which does not take into account the charge redistribution in the near-surface region of the SPR transducer [3,13,29]. The shift of the SPR curve to the large angles (Figure 4, inset), its broadening and the increase in the minimum value of the reflection intensity under resonance conditions are in good agreement with the assumption of the formation of a non-uniform layer of nanoparticles, the local environment of which differs somewhat from each other; however, the effect of an external static field also leads to similar effects according to ref. [30]. The size of a nanoparticle is comparable to the region in which the main part of the evanescent wave energy is concentrated, on the one hand, and is capable of changing the local configuration of the double electric layer, on the other. Thus, the adsorption of a "large" charged object changes the result of the superposition of electric fields caused by the charge on the transducer surface, the volume charge of the diffusion layer and on the surface of the nanoparticle, affecting the conditions for the excitation of the SPR. A more detailed description of this direction of SPR technology development can be found in the works [30–32]. For the purposes of this work, it is sufficient to establish the fact that positively charged Ag-NP&BPEI nanoparticles effectively bind to the surface of gold modified with thiocyanate. The specific features of SPR response obtained indicate that the acting force of the adsorption interaction is electrostatic attraction. This confirms the assumption made earlier in ref. [8,33] that as a result of gold modification with thiocyanate, negative charge centers are created in the near-surface region, fixed on the surface. Adsorption binding occurs due to ion exchange on the surface when small-radius counterions from the solution are replaced by large-size multicenter positively charged objects (proteins,

nanoparticles etc.); such a substitution reaction is always shifted toward the formation of a large-size counterion layer.

The recently invented wide-field Surface Plasmon Resonance Microscopy (wf-SPRM, [34–36]) was used in this work to directly visualize nanoparticles on a thiocyanate-modified gold surface. The advancing ability of the wf-SPRM platform among nanoparticle counting methods, argued in detail in ref. [37,38]. The concept of the plasmon scattering interferometry is follows. When an object appears on the propagation path of a surface wave (Surface Plasmon Polariton, SPP), a part of this wave is reflected back, and a part is scattered—depending on the size, shape and material of the object. Since all waves in the plane of the surface are coherent, this leads to the interference of the reflected, scattered and incident waves. The resulting interference pattern is actually of a microscopic size and can be easily detected by technical means of conventional optical microscopy [39–44]. In the present study this technique has been applied to visualize the adsorption of 60 nm silver NPs stabilized by the compounds with varying terminal functions groups (citrate, BPEI, PVP and PEG surfaces possessing different charge and hydrophobicity) on the SCN-modified gold surface.

As it was discussed above, Citrate, PEG and PVP stabilized silver NPs are negatively charged NPs, while branched BPEI-coated silver NPs are positively charged NPs at pH 5.5-6 (distilled water). As expected, the adsorption of NPs to the SCN-modified surface depends strongly on the type of coating charge. The typical results of adsorption of the positively charged BPEI-Ag NPs to SCN-modified surface are shown in Figure 5c, while the result of injection the negatively charged citrate stabilized NPs is presented in Figure 5b. Comparison of the images of the gold surface modified with thiocyanate (Figure 5a) with the images obtained after the injection of Ag-NP&CIT (Figure 5b), Ag-NP&PEG (similar to Figure 5a) and Ag-NP&PVP (similar to Figure 5a) suspensions clearly indicates that the process of adsorption of these particles on SCN-modified gold surface is not observed. The behavior of positively charged Ag-NP&BPEI nanoparticles showed the opposite effect: they are actively adsorbed on the gold surface modified with thiocyanate (Figure 5c).

Thiocionate modified Gold surface (**a**) | After injection of Ag-NP&CIT suspension (**b**) | After injection of Ag-NP&BPEI suspension (**c**)

Figure 5. Differential wf-SPRM images of SCN-modified gold surface in water (**a**) and the same surface after addition of 60 nm citrate stabilized Ag nanoparticles (**b**) or Ag-NP&BPEI suspension (**c**). Image size: 1900 × 1900 pixels (field of view is c.a. 0.9 × 0.9 mm^2). The measurements were carried out in static mode using an open-type cuvette (200 μL): the cuvette was filled with 140 μL of distilled water, to which 10 μL of nanoparticles with a concentration of 0.02 mg/mL were added. The measurements were performed at low ionic strength (distilled water, 55 μS/cm). The inset shows the optical image of nanoparticles caused by the processes of interference of surface waves of plasmon-polariton excitations.

4. Concluding Remarks

The findings obtained using different experimental approaches are consistent with the hypothesis made in ref. [8] that the gold surface modified with thiocyanate behaves as

a negatively charged object in processes drive by electrostatic interactions. The nature and mechanism of formation of such a charge still remain unclear. Possible explanations include the higher electronegativity of nitrogen and the stabilization of the S=C=N$^-$ tautomer upon formation of the sulfur bond with gold as well as potential participation of other ions in the formation of a thermodynamically stable surface structure. These issues still require detailed theoretical consideration.

For many practical purposes, like electrostatic immobilization of bioreceptors [5–7], such an interpretation of the SCN-modified gold surface as negatively charged is sufficient. Thus, from a simplified electrostatic analysis it can be concluded that the adsorption of charged objects on the SCN-modified surface is a spontaneous process electrostatically driven. This statement is in good agreement with the results of other authors concerning the interaction of positively charged BPEI with SiC or SiO_2 surfaces [45], where the charge is strictly localized and is not surrounded by small-radius counterions.

The situation becomes much more complicated when the adsorption of a "large" charged object occurs inside a double electric layer (the screening diffuse layer in distilled water is very wide and can be estimated by the Debye length): changes in both the surface charge (Stern layer) and the distribution of electric potential of the Gouy layer affect the conditions for the excitation and propagation of plasmon-polariton excitations. Thus, the detection of charged nanoparticles by SPR is a more complex issue which dependent on a broad range of facets. Therefore, in general adsorption on oppositely charged objects has to be analyzed not only as a function of the stationary surface charge distribution, but also as a function of the salt concentration in the medium (to estimate the thickness of double layer) and self-consistent interface electric fields [46]. And this is only if the effect of other forces driving adsorption reaction, such as van der Waals forces, hydrogen bonds, solvation effects, etc., can be neglected.

In this scenario, the electrostatically driven adsorption of Ag-NP&BPEI can be regarded as a good example to demonstrate the difference with conventional charge-free interface layers. The BPEI, as a cationic polyelectrolyte with a high content of Lewis base amines, can modify the electrical properties of the surface on which it is attached [47,48]. Although the initial adsorption is probably controlled by electrostatic attraction with a corresponding change in the optical parameters of the near-surface layer, the subsequent SPR response (Figure 4) is the result of mutual coordination of the surface charge localized on the nanoparticles and the surface, the spatial distribution of the electrical double layer, and the plasmon-polariton excitation itself. Modern approaches to analyze SPR data do not consider any processes involving charges or currents when formulating or analyzing the optical model of the system. The necessity of taking these effects into account and the limits of applicability of the standard classical approach without taking into account the charge redistribution process when analyzing the nanoparticle adsorption still await their understanding and theoretical justification. We hope that this work will contribute to the successful development of this direction.

Author Contributions: Conceptualization, B.A.S.; methodology, S.N., A.L. and B.A.S.; formal analysis and validation, B.A.S., A.L. and S.N.; investigation, B.A.S., A.L. and S.N.; data curation, A.L., B.A.S. and T.V.S.; writing—original draft preparation, B.A.S.; writing—review and editing, S.N., A.L. and B.A.S.; visualization, T.V.S.; project administration, B.A.S. All authors have read and agreed to the published version of the manuscript.

Funding: This work has received funding through the MSCA4Ukraine project (Grant ID 1119494), which is funded by the European Union under Marie Skłodowska-Curie Actions (MSCA), Horizon 2020.

Institutional Review Board Statement: Not applicable.

Informed Consent Statement: Not applicable.

Data Availability Statement: Data are available upon request.

Acknowledgments: The authors express their gratitude to Professor Vladimir Mirsky for support in the research and fruitful discussions.

Conflicts of Interest: The authors declare no conflict of interest.

References

1. Banica, F.-G. *Chemical Sensors and Biosensors: Fundamentals and Applications Chemical Sensors and Biosensors: Fundamentals and Applications*; John Wiley & Sons: Hoboken, NJ, USA, 2012.
2. *Handbook of Surface Plasmon Resonance*; Hardback; Schasfoort, R.B.M.: Oldenzaal, The Netherlands, 2017; p. 524, ISBN:978-1-78262-730-2. https://doi.org/10.1039/9781788010283.
3. Snopok, B. Biosensing under Surface Plasmon Resonance Conditions. In *21st Century Nanoscience—A Handbook Nanophotonics, Nanoelectronics, and Nanoplasmonics*; CRC Press: Boca Raton, FL, USA, 2020. https://doi.org/10.1201/9780429351617.
4. Boltovets, P.M.; Snopok, B.A. Measurement uncertainty in analytical studies based on surface plasmon resonance. *Talanta* **2009**, *80*, 466–472. https://doi.org/10.1016/j.talanta.2009.07.009.
5. Lvov, Y.; Decher, G.; Moehwald, H. Assembly, structural characterization, and thermal behavior of layer-by-layer deposited ultrathin films of poly(vinyl sulfate) and poly(allylamine)Click to copy article link. *Langmuir* **1993**, *9*, 481–486.
6. Snopok, B.A.; Goltsov, Y.G.; Kostyukevich, E.V.; Matkovskaja, L.A.; Shirshov, Y.M.; Venger, E.F. Self-assembled multilayer superstructures as immobilization support for bioreceptors. *Sens. Actuators B Chem.* **2003**, *95*, 336–343. https://doi.org/10.1016/S0925-4005(03)00536-7.
7. Boltovets, P.; Shinkaruk, S.; Vellutini, L.; Snopok, B. Self-tuning interfacial architecture for Estradiol detection by surface plasmon resonance biosensor. *Biosens. Bioelectron.* **2017**, *90*, 91–95. https://doi.org/10.1016/j.bios.2016.11.017.
8. Boltovets, P.M.; Snopok, B.A.; Shirshov, Y.M.; Dyachenko, N.S. Arranged protein layers for optoelectronic biosensor systems: Oriented protein immobilization on modified gold surface. *Rep. Natl. Acad. Sci. Ukr.* **2001**, *11*, 137–144.
9. Barbosa-Filho, O.; Monhemius, A.J. Leaching of gold in thiocyanate solutions—Part 1: Chemistry and thermodynamics. *Trans. Inst. Min. Metall.* **1994**, *103*, C105.
10. Ahsan, M.T.; Manny, F.; Hossain, M.; Miah, R.; Aziz, A.; Hasnat, M.A. Spontaneous immobilization of thiocyanate onto Au surface for the detection of uric acid in basic medium. *Surf. Interfaces* **2023**, *36*, 102599. ISSN 2468-0230. https://doi.org/10.1016/j.surfin.2022.102599.
11. Gong, J.; Li, Y.; Zhao, Y.; Wu, X.; Wang, J.; Zhang, G. Metal-free polymeric (SCN)n photocatalyst with adjustable bandgap for efficient organic pollutants degradation and Cr(VI) reduction under visible-light irradiation. *Chem. Eng. J.* **2020**, *402*, 126147.
12. Snopok, B.A.; Kostyukevych, K.V.; Beketov, G.V.; Zinio, S.A.; Shirshov, Y.M.; Venger, E.F. Biochemical passivation of metal surfaces for sensor application: Reactive annealing of polycrystalline gold films in hydrogen sulfide atmosphere. *Semicond. Phys. Quantum Electron. Optoelectron.* **2000**, *3*, 59–68. https://doi.org/10.15407/spqeo3.01.059.
13. Snopok, B.A.; Laroussi, A.; Cafolla, C.; Voïtchovsky, K.; Snopok, T.; Mirsky, V.M. Gold surface cleaning by etching polishing: Optimization of polycrystalline film topography and surface functionality for biosensing. *Surf. Interfaces* **2021**, *22*, 100818. https://doi.org/10.1016/j.surfin.2020.100818.
14. Mukhopadhyay, R. Surface plasmon resonance instruments diversify. *Anal. Chem.* **2005**, *77*, 313 A–317 A.
15. Zybin, A. Method for High-Resolution Detection of Nanoparticles on Two-Dimensional Detector Surfaces. Patent: US8587786B2.
16. Nizamov, S.; Mirsky, V.M. Wide-Field Surface Plasmon Resonance Microscopy for In-Situ Characterization of Nanoparticle Suspensions. In *In-Situ Characterization Techniques for Nanomaterials*; Kumar, C.S.S.R., Ed.; Springer: Berlin/Heidelberg, Germany, 2018. https://doi.org/10.1007/978-3-662-56322-9_3.
17. Sidorenko, I.; Nizamov, S.; Hergenröder, R.; Zybin, A.; Kuzmichev, A.; Kiwull, B.; Niessner, R.; Mirsky, V.M. Computer assisted detection and quantification of single adsorbing nanoparticles by differential surface plasmon microscopy. *Microchim. Acta* **2016**, *183*, 101–109.
18. Zboril, R.; Soukupová, J. Method of Immobilization of Silver Nanoparticles on Solid Substrate. US 9,505,027 B2, 29 November 2016.
19. Kim, K.G.; Kim, S.Y. Increase in Interfacial Adhesion and Electrochemical Charge Storage Capacity of Polypyrrole on Au Electrodes Using Polyethyleneimine. *Sci. Rep.* **2019**, *9*, 2169.
20. Sung, C.; Heo, Y. Porous Layer-by-Layer Films Assembled Using Polyelectrolyte Blend to Control Wetting Properties. *Polymers* **2021**, *13*, 2116.
21. Zucker, R.M.; Ortenzio, J.; Degn, L.L.; Lerner, J.M.; Boyes, W.K. Biophysical comparison of four silver nanoparticles coatings using microscopy, hyperspectral imaging and flow cytometry. *PLoS ONE* **2019**, *14*, e0219078.
22. Elgrishi, N.; Rountree, K.J.; McCarthy, B.D.; Rountree, E.S.; Eisenhart, T.T.; Dempsey, J.L. A Practical Beginner's Guide to Cyclic Voltammetry. *J. Chem. Educ.* **2018**, *95*, 197–206. https://doi.org/10.1021/acs.jchemed.7b00361.
23. Heinze, J. Cyclic Voltammetry—"Electrochemical Spectroscopy". New Analytical Methods (25). *Angew. Chem. Int. Ed.* **1984**, *23*, 831–847. https://doi.org/10.1002/anie.198408313.
24. Tsai, T.H.; Thiagarajan, S.; Chen, S.M. Green synthesized Au–Ag bimetallic nanoparticles modified electrodes for the aperometric detection of hydrogen peroxide. *J. Appl. Electrochem.* **2010**, *40*, 2071–2076.

25. Saw, E.N.; Grasmik, V.; Rurainsky, C.; Epple, M.; Tschulik, K. Electrochemistry at single bimetallic nanoparticles—Using nano impacts for sizing and compositional analysis of individual AgAu alloy nanoparticles. *Faraday Discuss*. **2016**, *193*, 327–338.
26. Nizamov, S.; Kasian, O.; Mirsky, V.M. Individual Detection and Electrochemically Assisted Identification of Adsorbed Nanoparticles by Using Surface Plasmon Microscopy. *Angew. Chem. Int. Ed.* **2016**, *55*, 7247.
27. Scherbahn, V.; Nizamov, S.; Mirsky, V.M. Toward Ultrasensitive Surface Plasmon Resonance Sensors. In *Label-Free Biosensing*; Springer Series on Chemical Sensors and Biosensors; Schöning, M., Poghossian, A., Eds.; Springer: Heidelberg, Germany, 2018; 16.
28. Laurinavichyute, V.K.; Nizamov, S.; Mirsky, V.M. Real time tracking of the early stage of electrochemical nucleation. *Electrochim. Acta* **2021**, *382*, 138278.
29. Snopok, B.A. Theory and Practical Application of Surface Plasmon Resonance for Analytical Purposes. *Theor. Exp. Chem.* **2012**, *48*, 283–306. https://doi.org/10.1007/s11237-012-9274-6.
30. Abayzeed, S.A.; Smith, R.J.; Webb, K.F.; Somekh, M.G.; See, C.W. Sensitive detection of voltage transients using differential intensity surface plasmon resonance system. *Opt. Express* **2017**, *25*, 31552–31567.
31. Lopatynskyi, A.M.; Lopatynska, O.G.; Guiver, M.D.; Poperenko, L.V.; Chegel, V.I. Factor of interfacial potential for the surface plasmon-polariton resonance sensor response. *Semicond. Phys. Quantum Electron. Optoelectron* **2008**, *11*, 329–336.
32. Laurinavichyute, V.K.; Nizamov, S.; Mirsky, V.M. The Role of Anion Adsorption in the Effect of Electrode Potential on Surface Plasmon Resonance Response. *ChemPhysChem* **2017**, *18*, 1552.
33. Boltovets, P.M.; Dyachenko, N.S.; Snopok, B.A.; Shirshov, Y.M.; Lampeka, Y.D. Protein-orientating structures: Thiocyanate layers as support for immobilization of bioreceptors. In Proceedings of the SPIE 4425, Selected Papers from the International Conference on Optoelectronic Information Technologies, Vinnytsia, Ukraine, 12 June 2001. https://doi.org/10.1117/12.429722.
34. Nizamov, S.; Dimchevska Sazdovska, S.; Mirsky, V.M. A review of optical methods for ultrasensitive detection and characterization of nanoparticles in liquid media with a focus on the wide field surface plasmon microscopy. *Anal. Chim. Acta* **2022**, *1204*, 339633.
35. Scherbahn, V.; Nizamov, S.; Mirsky, V.M. Plasmonic detection and visualization of directed adsorption of charged single nanoparticles to patterned surfaces. *Microchim. Acta* **2016**, *183*, 2837–2845.
36. Sun, X.; Wang, X.; Wang, C.; Sun, A.; Liu, H.; Wang, F.; Cao, Y.; Wang, S.; Lu, X. Chengjun Huang. Effects of nanoparticle sizes, shapes, and permittivity on plasmonic imaging. *Opt. Express* **2022**, *30*, 6051–6060.
37. Nizamov, S.; Scherbahn, V.; Mirsky, V.M. Detection and Quantification of Single Engineered Nanoparticles in Complex Samples Using Template Matching in Wide-Field Surface Plasmon Microscopy. *Anal. Chem.* **2016**, *88*, 10206–10214. https://doi.org/10.1021/acs.analchem.6b02878.
38. Nizamov, S.; Scherbahn, V.; Mirsky, V.M. Detection of Single Sub-Micrometer Objects of Biological or Technical Origin Using Wide Field Surface Plasmon Microscopy. *Proceedings* **2017**, *1*, 788. https://doi.org/10.3390/proceedings1080788.
39. Nizamov, S.; Scherbahn, V.; Mirsky, V.M. Ionic Referencing in Surface Plasmon Microscopy: Visualization of the Difference in Surface Properties of Patterned Monomolecular Layers. *Anal. Chem.* **2017**, *89*, 7, 3873–3878.
40. Demetriadou, A.; Kornyshev, A. A Principles of nanoparticle imaging using surface plasmons. *New J. Phys.* **2015**, *17*, 013041.
41. Maley, A.M.; Lu, G.J.; Shapiro, M.G.; Corn, R.M. Characterizing Single Polymeric and Protein Nanoparticles with Surface Plasmon Resonance Imaging Measurements. *ACS Nano* **2017**, *11*, 744–745.
42. Sharar, N.; Wüstefeld, K.; Talukder, R.M.; Skolnik, J.; Kaufmann, K.; Giebel, B.; Börger, V.; Nolte, F.; Watzl, C.; Weichert, F.; et al. The Employment of the Surface Plasmon Resonance (SPR) Microscopy Sensor for the Detection of Individual Extracellular Vesicles and Non-Biological Nanoparticles. *Biosensors* **2023**, *13*, 472. https://doi.org/10.3390/bios13040472
43. Al-Bataineh, Q.M.; Telfah, A.D.; Tavares, C.J.; Hergenröder, R. Modeling and analysis of discrete particle detection in wide-field surface plasmon resonance microscopy. *Sensors and Actuators A: Physical*. **2024**, *370*, 115266. https://doi.org/10.1016/j.sna.2024.115266
44. Snopok, B.A.; Snopok, O.B. Nanoscale–Specific Analytics: How to Push the Analytic Excellence in Express Analysis of CBRN. In *Advanced Nanomaterials for Detection of CBRN*; NATO Science for Peace and Security Series A: Chemistry and Biology Bonča, J., Kruchinin, S., Eds.; Springer: Dordrecht, Germany, 2020. https://doi.org/10.1007/978-94-024-2030-2_13.
45. Mészáros, R.; Thompson, L.; Bos, M.; De Groot, P. Adsorption and electrokinetic properties of polyethylenimine on silica surfaces. *Langmuir* **2002**, *18*, 6164–6169.
46. Luque-Caballero, G.; Martín-Molina, A.; Quesada-Pérez, M. Polyelectrolyte adsorption onto like-charged surfaces mediated by trivalent counterions: A Monte Carlo simulation study. *J. Chem. Phys.* **2014**, *140*, 174701.
47. Yang, X.; Ying, Z.; Yang, Z.; Xu, J.-R.; Wang, W.; Wang, J.; Wang, Z.; Yao, L.; Yan, B.; Ye, J. Light-Promoted Electrostatic Adsorption of High-Density Lewis Base Monolayers as Passivating Electron-Selective Contacts. *Adv. Sci.* **2021**, *8*, 2003245. https://doi.org/10.1002/advs.202003245.
48. Barick, P.; Saha, B.P.; Mitra, R.; Joshi, S.V. Effect of concentration and molecular weight of poly-ethylenimine on zeta potential, isoelectric point of nanocrystalline silicon carbide in aqueous and ethanol medium. *Ceram. Int.* **2015**, *41 Pt B*, 4289–4293. ISSN 0272-8842. https://doi.org/10.1016/j.ceramint.2014.11.115/.